A Dynamic Directed Transfer Function For Brain Functional Network Based Feature Extraction

Mingai Li
Beijing University of Technology
Na Zhang (861737447@qq.com)
Beijing University of Technology

Research

Keywords: directed transfer function, feature extraction, motor imagery electroencephalogram, brain functional network, graph theory

Posted Date: September 20th, 2021

DOI: https://doi.org/10.21203/rs.3.rs-470657/v1

Version of Record: A version of this preprint was published at Brain Informatics on March 18th, 2022. See the published version at https://doi.org/10.1186/s40708-022-00154-8.

A dynamic Directed Transfer Function for Brain Functional Network based Feature Extraction

Mingai Li[a,b,c] and Na Zhang[a*]

[a] *Faculty of Information Technology, Beijing University of Technology, Beijing 100124, China;*

[b] *Beijing Key Laboratory of Computational Intelligence and Intelligent System, Beijing, 100124, China;*

[c] *Engineering Research Center of Digital Community, Ministry of Education, Beijing 100124, China*

**Correspondence:861737447@qq.com*

Abstract

Directed transfer function (DTF) is good at characterizing the pairwise interactions from the whole brain network and has been applied for discriminating different motor imagery (MI) tasks. Considering the fact that MI electroencephalogram signals are more non-stationary in frequency domain than in time domain, and the activated intensities of α band (8-13Hz) and β band (13-30Hz, with β_1(13-21Hz) and β_2(21-30Hz) included) have considerable differences for different subjects, a dynamic DTF (DDTF) with variable model order and frequency band is proposed to construct the brain functional networks (BFNs), whose information flows and outflows are further calculated as network features and evaluated by support vector machine. Extensive experiments are conducted based on a public BCI competition dataset and a real-world dataset, the highest recognition rate achieve 100% and 86%, respectively. The experimental results suggest that DDTF can reflect the dynamic evolution of BFN, the best subject-based DDTF appears in one of four frequency subbands (α, β, β_1, β_2) for discrimination of MI tasks and is much more related to the current and previous states. Besides, DDTF is superior compared to granger causality-based and traditional feature extraction methods, the t-test and Kappa values show its statistical significance and high consistency as well.

Keywords: directed transfer function, feature extraction, motor imagery electroencephalogram, brain functional network, graph theory

1. Introduction

Brain-computer interface (BCI) is a technology that allows people with healthy bodies or motor impairments to communicate with external environment through their brains' activity without the assistance of peripheral nerves and muscles [1-2]. Motor imagery (MI) is commonly used in BCI. Complex motor imagery can activate scattered areas of cortex. MI-EEG is a multichannel and time-frequency signal with spatial distribution features. The

key to improve recognition accuracy is how to effectively use these characteristics of MI-EEG for feature extraction [3].

In the past years, a variety of feature extraction methods have been used in the process of classifying mental tasks. Common spatial pattern (CSP) is one of the most popular and efficient algorithms which is particularly renowned for the high classification rates, notably during BCI competitions [4-6]. However, the classical CSP also has its limitations that it is sensitive to noise, overfitting and individual variability. To tackle these issues, a series of CSP-based methods have been proposed, including 'analytic signal'-based CSP(ACSP) [6], correlation-based channel selection common spatial pattern(CCS-RCSP)[7], common complex-spatio spectral pattern(CCSSP) [8] and complex common spatial patterns(CCSPs) [9]. The variants of CSP methods make full of the multi-channel and spatial distribution characteristics of MI-EEG for feature extraction and achieve preferable classification accuracies. Regretfully, information transfer and flow between channels do not get much attention. In fact, EEG researchers have tended to reveal that during the performance of even simple motor or cognitive tasks, many different functional areas widely scattered over the brain are mutually interconnected and exchange their information with one another, thus making it hard to isolate one or two regions where the activity takes place [10]. Physiologically speaking, when humans are involved in a motor task, our brains function as a complex network with the interactions of specialized, spatially distributed but functionally linked brain regions [11-15], contributing to the related brain functions. Therefore, it is an important strategy for ameliorating MI-EEG feature extraction to discover and use information flow between multi-channel EEG signals.

Recent years have witnessed that many researchers topologically characterize brain functional network by employing a mathematical framework called graph theory [16-18]. In graph theory, a network is defined as a graph formed by a set of nodes interconnected by edges [19]. Nodes in large-scale brain functional networks usually represent regions of interest (ROIs) or EEG electrodes, while links represent functional connectivity [20]. Generally, we can construct directed or undirected brain functional networks depending on adopting symmetric or asymmetric metrics of coupling between two signals. Anyway, in order to obtain abundant and exact properties, directed brain functional network is employed in this study. One of the commonly used techniques to construct a directed brain functional network is Granger causality (GC), which is aimed to illuminate casual temporal relations and directional nature of information flow for a pair of EEG channels. The basic notion of GC was originally conceived by Wiener [23], later adopted and formalized by Granger in the form of linear regression model. Granger's concept of causality has received a lot of people's attention and has been extensively employed in the field of economics and later adapted to neuroscience [24]. Since spectral properties are significant in biomedical signal analysis, extension of the concept to the frequency domain representation of time series was formulated by Geweke [25]. Although the above methods had lots of applications in many areas, it should be noted that they estimated directional information flow through bivariate approaches

without using the whole covariance structure for a multivariate system. Unfortunately, it was reported that bivariate measures in certain cases could potentially give spurious connections and misleading results especially when some signals are fed from common channel sources, as is very likely in neurobiological systems [26].

To meet the demands, a full multivariate estimator, i.e., directed transfer function (DTF), was proposed to overcome the limitations of bivariate autoregressive methods and characterize directional connectivity as well as spectral properties of the interactions between any given pair of brain signals, requiring only one multivariate autoregressive (MVAR) model to be estimated simultaneously from all the EEG time recordings [27-28]. That is, all signals are regarded as members of one system and their mutual influences (not limited to pairwise connections) are taken into account. Subsequently, many DTF-based methods were developed. Ding M et al. [29] proposed a short time directed transfer function (SDTF), in which the entire data was divided into short overlapping time intervals for computation of DTF measure on each interval. Ginter J et al. [30] and Yi W et al. [31] calculated SDTF to exhibit the casual relations of brain functional networks caused by motor imagery afterwards. Korzeniewska A [32] first introduced a full frequency Directed Transfer Function (ffDTF) in which the normalization of DTF is performed over the full frequency band, then dDTF [32] was derived by multiplying ffDTF by partial coherence to only show direct connections while DTF and ffDTF reveal both direct and indirect connections. Billinger M [33] showed the possibility of reliable classification of MI tasks through ffDTF and dDTF. Later in [34], dDTF was applied to power spectral density based feature extraction. Adaptive Directed Transfer Function (ADTF) was originally proposed by Wilke C et al. [35] for abnormal physiological signals, such as those during epileptic seizures. The authors established time-varying coefficient matrices by the Kalman filter algorithm, constructed MVAAR models and got time-varying brain functional networks. In the following years, ADTF was also used in the construction of time-varying brain function networks of other EEG signals. Li F et al. [36-37] used ADTF to investigate the time-varing P300 network patterns and to evaluate time-varing MI-EEG functional networks as well as observe the MI information processing in different stages. Wang D et al. [38] presented a novel wavelet-based directed transfer function (WDTF) method by combining the wavelet decomposition and the directed transfer function (DTF) algorithm for patient-specific seizure detection.

To sum up, DTF and its extended methods have successively been applied to construct brain functional networks and shown their effectiveness for different EEG signals. It is a potential problem that how to grasp the activated characteristics of MI-EEG signals to further improve DTF and find effective feature parameters to identify MI tasks. In order to fully represent the variation characteristics of MI-EEG in frequency domain, we will present a dynamic DTF, named as DDTF. The experimental research on publicly available MI-EEG data from BCI competition and real acquisition data from real-world experiment suggests this metric not only extracts effective information but also achieves a high classification accuracy while only one or two order frequency domain model is used to select the best frequency band

and calculate DDTF, demonstrating the adaptive and dynamic characteristics of MI-EEG.

The rest of the paper is organized as follows: in section 2, the proposed method for brain functional network based feature extraction is described in detail. Experimental research is performed in section 3. Section 4 provides the discussions and conclusions are drawn in the final section.

2. Methods

By adaptive selection of the frequency band and model order *m*, DTF is developed to generate DDTF, which is applied to brain functional network based feature extraction, the main steps are as follows: preprocessing of MI-EEG Signals, brain functional network construction based on DDTF, definition of characteristic parameters and construction of a feature vector. The support vector machine (SVM) is used to evaluate the feature vectors and get the best accuracies. The algorithm of the proposed DDTF for brain functional network based feature extraction is demonstrated at the end of this section.

2.1 Preprocessing of MI-EEG Signals

Suppose that $\boldsymbol{x}_0(t) = \left[x_{01}(t), x_{02}(t), \cdots, x_{0N_0}(t)\right]^T \in R^{N_0 \times K_0}$ represents the original MI-EEG signals, where N_0 and K_0 refer to the number of total channels and sample points, respectively.

Step1: Common average removal (CAR) filtering.

$\boldsymbol{x}_0(t)$ is spatially filtered with the CAR filter at first and the filtered signal is expressed as

$$\boldsymbol{x}_1(t) = \left[x_{11}(t), x_{12}(t), \cdots, x_{1N_0}(t)\right]^T \in R^{N_0 \times K_0} \tag{1}$$

Step2: Optimal sample interval selection.

The optimal sample interval [a,b] is selected with the most obvious event-related desynchronization (ERD)/ event-related synchronization (ERS) physiological phenomenon and MI-EEG signals in this time period are regarded as

$$\boldsymbol{x}_2(t) = \left[x_{21}(t), x_{22}(t), \cdots, x_{2N_0}(t)\right]^T \in R^{N_0 \times K} \tag{2}$$

where $K = b - a + 1$.

Step3: Bandpass filtering

The important information in EEG signals is often hidden in frequency with respect to allied cognitive tasks [39] and it is generally accepted that most of the motor imagine-related EEG signals are coded in the frequency band of 8-30 Hz [40]. What's more, the β band

(13-30Hz) ,with β_1 or lower β band (13-21Hz) and β_2 or higher β band (21-30Hz) included, has been reported to be good physiological predictors during motor imagery tasks comparing to other frequency bands [41]. This information is significant, as it has been verified that interdependency at different frequency ranges may own distinct physiological functions, e.g., [42]. At this point, $\boldsymbol{x}_2(t)$ is bandpass filtered to α band and β band (β_1 and β_2 band if necessary) and the filtered signals are later described as

$$\begin{cases} \boldsymbol{x}_2^{\alpha}(t) = \left[x_{21}^{\alpha}(t), x_{22}^{\alpha}(t), \cdots, x_{2N_0}^{\alpha}(t)\right]^T \in R^{N_0 \times K} \\ \boldsymbol{x}_2^{\beta}(t) = \left[x_{21}^{\beta}(t), x_{22}^{\beta}(t), \cdots, x_{2N_0}^{\beta}(t)\right]^T \in R^{N_0 \times K} \\ \boldsymbol{x}_2^{\beta_1}(t) = \left[x_{21}^{\beta_1}(t), x_{22}^{\beta_1}(t), \cdots, x_{2N_0}^{\beta_1}(t)\right]^T \in R^{N_0 \times K} \\ \boldsymbol{x}_2^{\beta_2}(t) = \left[x_{21}^{\beta_2}(t), x_{22}^{\beta_2}(t), \cdots, x_{2N_0}^{\beta_2}(t)\right]^T \in R^{N_0 \times K} \end{cases}$$

(3)

Step4: Channel selection

Considering the computational complexity and feature information redundancy, N channels are selected to cover as many brain regions as possible in the premise of guaranteeing their asymmetries, the signals after channel selection are written as $\boldsymbol{x}_3^{\alpha}(t) = [x_{31}^{\alpha}(t), x_{32}^{\alpha}(t), \cdots, x_{3N}^{\alpha}(t)] \in R^{\mathrm{N} \times K}, \boldsymbol{x}_3^{\beta}(t) = \left[x_{31}^{\beta}(t), x_{32}^{\beta}(t), \cdots, x_{3N}^{\beta}(t)\right] \in R^{\mathrm{N} \times K}$, $\boldsymbol{x}_3^{\beta_1}(t) = \left[x_{31}^{\beta_1}(t), x_{32}^{\beta_1}(t), \cdots, x_{3N}^{\beta_1}(t)\right] \in R^{\mathrm{N} \times K}$, $\boldsymbol{x}_3^{\beta_2}(t) = \left[x_{31}^{\beta_2}(t) \quad , \quad x_{32}^{\beta_2}(t), \cdots, x_{3N}^{\beta_2}(t)\right]$ and later rewritten as

$$\begin{cases} \boldsymbol{x}^{\alpha}(t) = [x_1^{\alpha}(t), x_2^{\alpha}(t), \cdots, x_N^{\alpha}(t)]^T \in R^{N \times K} \\ \boldsymbol{x}^{\beta}(t) = \left[x_1^{\beta}(t), x_2^{\beta}(t), \cdots, x_N^{\beta}(t)\right]^T \in R^{N \times K} \\ \boldsymbol{x}^{\beta_1}(t) = \left[x_1^{\beta_1}(t), x_2^{\beta_1}(t), \cdots, x_N^{\beta_1}(t)\right]^T \in R^{N \times K} \\ \boldsymbol{x}^{\beta_2}(t) = \left[x_1^{\beta_2}(t), x_2^{\beta_2}(t), \cdots, x_N^{\beta_2}(t)\right]^T \in R^{N \times K} \end{cases}$$

(4)

2.2 The proposed dynamic DTF (DDTF)

In this subsection, DTF is improved, named as DDTF, in which the model order and frequency band are changing and adaptively selected by recognition rates. The detailed introduction takes α band for example.

Step1: Let us consider a multivariate autoregressive model (MVAR) in which the present state of MI-EEG signals can be approximated by a weighted sum of both its past p_α samples and the p_α previous values of other channels plus a random noise series as follows:

$$\boldsymbol{x}^{\alpha}(t) = \sum_{r=1}^{p_\alpha} \boldsymbol{A}^{\alpha}(r)\boldsymbol{x}^{\alpha}(t-r) + \boldsymbol{e}^{\alpha}(t) \tag{5}$$

where $\boldsymbol{e}^{\alpha}(t) = [e_1^{\alpha}(t), e_2^{\alpha}(t), \cdots, e_N^{\alpha}(t)]^T$ is the estimation error which is a multivariate

uncorrelated white noise sequence with zero mean. $\boldsymbol{x}^{\alpha}(t-r)=[x_1^{\alpha}(t-r),x_2^{\alpha}(t-r),\cdots,x_N^{\alpha}(t-r)]^T$ is an $N\times1$ vector of $\boldsymbol{x}(t)$ at a time lag 'r'. $\boldsymbol{A}^{\alpha}(1),\boldsymbol{A}^{\alpha}(2),\cdots,\boldsymbol{A}^{\alpha}(\mathrm{r})$ are the $N\times N$ matrices of coefficient matrices, e.g., $\boldsymbol{A}^{\alpha}(r)$ is a matrix describing the time-lagged influences of $\boldsymbol{x}^{\alpha}(t-r)$ on $\boldsymbol{x}^{\alpha}(t)$. Assume each element of the matrix $\boldsymbol{A}^{\alpha}(r)$ is denoted as a_{uv}^{α}, the coefficient matrix can be set as $\mathbf{A}^{\alpha}(\mathrm{r})=\begin{pmatrix}a_{11}^{\alpha}(r) & \cdots & a_{1N}^{\alpha}(r)\\ \vdots & \ddots & \vdots\\ a_{N1}^{\alpha}(r) & \cdots & a_{NN}^{\alpha}(r)\end{pmatrix}$, the off-diagonal parts $a_{uv}^{\alpha}(r),u\neq v$ quantify time-lagged influences between different EEG signals $x_u^{\alpha}(t)$ and $x_v^{\alpha}(t)$. The model coefficients can be get iteratively so as to minimize the error between the actual values (measured) and the predicted ones. p_{α} is the model order which denotes the maximum time lag used to disclose the influences of past values on the current state, the optimal order of the model is determined by the Schwarz Bayesian Criterion(SBC) [43] and is used for the MVAR model fitting to the MI-EEG data.

Step2: Once the MVAR model is fully constructed, the dynamic spectral analysis is performed based on Fourier transform. The $\boldsymbol{B}^{m_{\alpha}}(f)$, which has a varying order m_{α}, is defined as follows:

$$\boldsymbol{B}^{m_{\alpha}}(f)=-\sum_{r=0}^{m_{\alpha}}\boldsymbol{A}^{\alpha}(r)e^{-j2\pi fr\Delta t},m_{\alpha}=1,2,\cdots,p_{\alpha} \tag{6}$$

with $\boldsymbol{B}^{0}(f)=-\mathrm{I}$ (I being the identity matrix). Δt is the temporal interval between two samples, j represents the imagery unit, and we have

$$\boldsymbol{B}^{m_{\alpha}}(f)\boldsymbol{X}^{\alpha}(f)=\boldsymbol{E}^{\alpha}(f) \tag{7}$$

where $\boldsymbol{X}^{\alpha}(f)$ and $\boldsymbol{E}^{\alpha}(f)$ are the transforms of $\boldsymbol{x}^{\alpha}(\mathrm{t})$ and $\boldsymbol{e}^{\alpha}(\mathrm{t})$, respectively.

Step 3: Eq. (7) can be rewritten as follows:

$$\boldsymbol{X}^{\alpha}(f)=[\boldsymbol{B}^{m_{\alpha}}(f)]^{-1}\boldsymbol{E}^{\alpha}(f)=\boldsymbol{H}^{m_{\alpha}}(f)\boldsymbol{E}^{\alpha}(f) \tag{8}$$

Here $\boldsymbol{H}^{m_{\alpha}}(f)$ is called the transfer matrix of the system, f denotes frequency. Then, based on elements of the transfer matrix $\boldsymbol{H}^{m_{\alpha}}(f)$, the DDTF from channel s to channel l at frequency f is defined as:

$$[\theta_{ls}^{m_{\alpha}}(f)]^2=\left|H_{ls}^{m_{\alpha}}(f)\right|^2 \tag{9}$$

where $H_{ls}^{m_{\alpha}}(f)$ is the element in the lth row of column s of transfer matrix $\boldsymbol{H}^{m_{\alpha}}(f)$. In addition, a normalization procedure is executed through dividing $[\theta_{ls}^{m_{\alpha}}(f)]^2$ by the squared sum of all elements in the relevant row as follows:

$$[\gamma_{ls}^{m_{\alpha}}(f)]^2=\frac{[\theta_{ls}^{m_{\alpha}}(f)]^2}{\sum_{q=1}^{N}[\theta_{lq}^{m_{\alpha}}(f)]^2} \tag{10}$$

which describes the ratio of influence from channel s to channel l with respect to the joint influence from all the other channels (to channel l) with a value between 0 to 1. Value close to 1 reveals that the fraction of channel s being present in channel l is very high while value

close to 0 shows channel *s* almost makes no contributions to channel *l*.

Step4: To get the mean value of Eq. (10) under different frequencies, the accumulation over α band is applied:

$$\overline{\Upsilon_{ls}^{m_\alpha}} = \frac{\sum_{f=f_1}^{f_2}[\gamma_{ls}^{m_\alpha}(f)]^2}{f_2-f_1+1} \tag{11}$$

Here f_1, f_2 equal to 8 and 13Hz (the lower and upper bound of α band), respectively. Perform the same steps for $\boldsymbol{x}^{\beta}(t), \boldsymbol{x}^{\beta_1}(t)$, $\boldsymbol{x}^{\beta_2}(t)$ and we get

$$\begin{cases} \overline{\Upsilon_{ls}^{m_\beta}} = \frac{\sum_{f=f_2}^{f_4}\left[\gamma_{ls}^{m_\beta}(f)\right]^2}{f_4-f_2+1} \\ \overline{\Upsilon_{ls}^{m_{\beta_1}}} = \frac{\sum_{f=f_2}^{f_3}\left[\gamma_{ls}^{m_{\beta_1}}(f)\right]^2}{f_3-f_2+1} \\ \overline{\Upsilon_{ls}^{m_{\beta_2}}} = \frac{\sum_{f=f_3}^{f_4}[\gamma_{ls}^{m_{\beta_2}}(f)]^2}{f_4-f_3+1} \end{cases} \tag{12}$$

where f_3, f_4 are 21 and 30Hz, respectively.

2.3 Brain functional network construction based on DDTF

$\overline{\Upsilon_{ls}^{m_\alpha}}$ reveals the direction and strength between two channels in the total α band. For example, $\overline{\Upsilon_{12}^{m_\alpha}}$ represents the connection intensity from channel 2 to channel 1 and vice versa. The brain functional network of α band then can be constructed with EEG electrodes as nodes and $\overline{\boldsymbol{\Upsilon}^{m_\alpha}}$, the adjacency matrix(AM), as links between channels. Similarly, brain functional networks of β, β_1 and β_2 band can also be constructed.

2.4 Definition of characteristic parameters

Characteristic parameters are obtained according to the brain functional networks and adjacency matrices. Given channel g (g=1,2, ⋯ ,N) for example, the feature matrix $\overline{\boldsymbol{\Upsilon}^{m_\alpha}}, \overline{\boldsymbol{\Upsilon}^{m_\beta}}, \overline{\boldsymbol{\Upsilon}^{m_{\beta_1}}}, \overline{\boldsymbol{\Upsilon}^{m_{\beta_2}}}$ are summed up by the gth row to acquire the information of inflow to channel g:

$$\begin{cases} IN^{m_\alpha}(g) = \sum_{s=1}^{N} \overline{\Upsilon_{gs}^{m_\alpha}} \\ IN^{m_\beta}(g) = \sum_{s=1}^{N} \overline{\Upsilon_{gs}^{m_\beta}} \\ IN^{m_{\beta_1}}(g) = \sum_{s=1}^{N} \overline{\Upsilon_{gs}^{m_{\beta_1}}} \\ IN^{m_{\beta_2}}(g) = \sum_{s=1}^{N} \overline{\Upsilon_{gs}^{m_{\beta_2}}} \end{cases} \tag{13}$$

As a logical sequence, the outflow from channel g is obtained through summing up the adjacency matrix by the gth column as follows:

$$\begin{cases} OUT^{m_\alpha}(g) = \sum_{l=1}^{N} \overline{\Upsilon_{lg}^{m_\alpha}} \\ OUT^{m_\beta}(g) = \sum_{l=1}^{N} \overline{\Upsilon_{lg}^{m_\beta}} \\ OUT^{m_{\beta_1}}(g) = \sum_{l=1}^{N} \overline{\Upsilon_{lg}^{m_{\beta_1}}} \\ OUT^{m_{\beta_2}}(g) = \sum_{l=1}^{N} \overline{\Upsilon_{lg}^{m_{\beta_2}}} \end{cases} \tag{14}$$

Inflow characterizes the sum of information received by a particular destination channel g from other channels while outflow describes gross messages transmitted from the given source node g to the rest of the network. Both explore the information interaction processes between specific areas of the brain and other regions.

Furthermore, the inflow and outflow are combined to define information flow (similarly, we take the channel g as an example):

$$\begin{cases} IF^{m_\alpha}(g) = \frac{OUT^{m_\alpha}(g)}{IN^{m_\alpha}(g)} \\ IF^{m_\beta}(g) = \frac{OUT^{m_\beta}(g)}{IN^{m_\beta}(g)} \\ IF^{m_{\beta_1}}(g) = \frac{OUT^{m_{\beta_1}}(g)}{IN^{m_{\beta_1}}(g)} \\ IF^{m_{\beta_2}}(g) = \frac{OUT^{m_{\beta_2}}(g)}{IN^{m_{\beta_2}}(g)} \end{cases} \tag{15}$$

Information flow indicates the role of channel g playing in the process of information transmission. The larger information flow is, the greater contribution g has to other channels. Conversely, it means that there is barely no or very little info from channel g when the value is approaching to 0.

2.5 Construction of a feature vector

Let's take α band for example, there is an $OUT^{m_\alpha}(g)$ and $IF^{m_\alpha}(g)$ for each channel g, $\boldsymbol{OUT}^{m_\alpha}$ and $\boldsymbol{IF}^{m_\alpha}$ can be obtained when the features related to all the N channels are assembled,namely, $\boldsymbol{OUT}^{m_\alpha} = [OUT^{m_\alpha}(1), OUT^{m_\alpha}(2), \cdots, OUT^{m_\alpha}(g), \cdots, OUT^{m_\alpha}(N)] \in R^{1\times N}$, $\boldsymbol{IF}^{m_\alpha} = [IF^{m_\alpha}(1), IF^{m_\alpha}(2), \cdots, IF^{m_\alpha}(g), \cdots, IF^{m_\alpha}(N)] \in R^{1\times N}$, where N means the number of selected channels. They are fused in serial to form the network eigenvector of α band, namely $\boldsymbol{F}^{m_\alpha}$:

$$\boldsymbol{F}^{m_\alpha} = [\boldsymbol{IF}^{m_\alpha}, \boldsymbol{OUT}^{m_\alpha}] \in R^{1\times 2N} \tag{16}$$

Analogously, feature vectors of β, β_1 or β_2 band can be acquired as follows:

$$\begin{cases} \boldsymbol{F}^{m_\beta} = [\boldsymbol{IF}^{m_\beta}, \boldsymbol{OUT}^{m_\beta}] \in R^{1\times 2N} \\ \boldsymbol{F}^{m_{\beta_1}} = [\boldsymbol{IF}^{m_{\beta_1}}, \boldsymbol{OUT}^{m_{\beta_1}}] \in R^{1\times 2N} \\ \boldsymbol{F}^{m_{\beta_2}} = [\boldsymbol{IF}^{m_{\beta_2}}, \boldsymbol{OUT}^{m_{\beta_2}}] \in R^{1\times 2N} \end{cases} \tag{17}$$

After this process, feature vectors at a characteristic frequency for those directed interconnections are regarded as the input vectors to the SVM classifier to discriminate different motor imagery tasks.

2.6 Feature evaluation by SVM

Given each m_α, we have corresponding features $\boldsymbol{F}^{m_\alpha}$ and accuracies Acc^{m_α}. Similarly, $\boldsymbol{F}^{m_\beta}$ and Acc^{m_β} can be obtained when MI-EEG signals are filtered to β band. As is said before, motor imagery response frequency bands are not consistent for each individual person. Therefore, it is of vital importance to find subject-specific frequency band, so accuracies in α band and β band are compared. Suppose Acc^{m_α} are higher than Acc^{m_β}, it means α band is the final frequency band we are seeking for. Instead, the best classification accuracy is hidden in β band. Filter MI-EEG signals to β_1 (13-21Hz) and β_2 band (21-30Hz), repeat the above operations and the best accuracy as well as frequency band can ultimately be acquired.

The DDTF Algorithm for brain functional network based feature extraction is as follows:

Input: MI-EEG signals $\boldsymbol{x}_0(t)$
01. Preprocessing of MI-EEG signals Step 1. Common average removal (CAR) filtering Step 2. Optimal sample interval selection Step 3. Bandpass filter to α (8-13Hz) and β band (13-30Hz) Step 4. Channel selection, get $\boldsymbol{x}^\alpha(t)$ and $\boldsymbol{x}^\beta(t)$
02. Adjacency matrix calculation based on DDTF Step 1. MVAR model fitting to $\boldsymbol{x}^\alpha(t)$ and $\boldsymbol{x}^\beta(t)$, respectively Step 2. Calculate $\boldsymbol{B}^{m_\alpha}(f)$ and $\boldsymbol{B}^{m_\beta}(f)$ using Equation (6) Step 3. Calculate DDTF and adjacency matrix of $[\theta_{ls}^{m_\alpha}(f)]^2$, $[\theta_{ls}^{m_\beta}(f)]^2$ and $\overline{\boldsymbol{Y}^{m_\alpha}}$, $\overline{\boldsymbol{Y}^{m_\beta}}$ using Equation (8) to (12
03. Definition of characteristic parameters Step 1. Extract the features of inflow $IN^{m_\alpha}(g)$ and $IN^{m_\beta}(g)$ by Equation (13) Step 2. Extract the features of outflow $OUT^{m_\alpha}(g)$ and $OUT^{m_\beta}(g)$ by Equation (14) Step 3. Extract the features of information flow $IF^{m_\alpha}(g)$ and $IF^{m_\beta}(g)$ by Equation (15)
04. Construction of a feature vector Obtain $\boldsymbol{OUT}^{m_\alpha}$, $\boldsymbol{IF}^{m_\alpha}$ and $\boldsymbol{OUT}^{m_\beta}$, $\boldsymbol{IF}^{m_\beta}$, yield feature vector $\boldsymbol{F}^{m_\alpha}$ and $\boldsymbol{F}^{m_\beta}$
05. Feature evaluation by SVM Compare Acc^{m_α} with Acc^{m_β}
If Acc^{m_α} are higher than Acc^{m_β}
Output: the best accuracy of α band, i.e., α^{ba}
Else If Acc^{m_α} are lower than Acc^{m_β}

01. Preprocessing of MI-EEG signals

Step 1. Common average removal (CAR) filtering

Step 2. Optimal sample interval selection

Step 3. Bandpass filter to β_1 (13-21Hz) and β_2 band (21-30Hz)

Step 4. Channel selection, get $\boldsymbol{x}^{\beta_1}(t)$ and $\boldsymbol{x}^{\beta_2}(t)$

02. Adjacency matrix calculation based on DDTF

Step 1. MVAR model fitting to $\boldsymbol{x}^{\beta_1}(t)$ and $\boldsymbol{x}^{\beta_2}(t)$, respectively

Step 2. Calculate $\boldsymbol{B}^{m_{\beta_1}}(f)$ and $\boldsymbol{B}^{m_{\beta_2}}(f)$ using Equation (6)

Step 3. Calculate DDTF and adjacency matrix of $[\theta_{ls}^{m_{\beta_1}}(f)]^2$, $[\theta_{ls}^{m_{\beta_2}}(f)]^2$ and $\overline{\boldsymbol{\Upsilon}^{m_{\beta_1}}}$, $\overline{\boldsymbol{\Upsilon}^{m_{\beta_2}}}$ using Equation (8) to (12)

03. Definition of characteristic parameters

Step 1. Extract the features of inflow $IN^{m_{\beta_1}}(g)$ and $IN^{m_{\beta_2}}(g)$ by Equation (13)

Step 2. Extract the features of outflow $OUT^{m_{\beta_1}}(g)$ and $OUT^{m_{\beta_2}}(g)$ by Equation (14)

Step 3. Extract the features of information flow $IF^{m_{\beta_1}}(g)$ and $IF^{m_{\beta_2}}(g)$ by Equation (15)

04. Construction of a feature vector

Obtain $\boldsymbol{OUT}^{m_{\beta_1}}, \boldsymbol{IF}^{m_{\beta_1}}$ and $\boldsymbol{OUT}^{m_{\beta_2}}, \boldsymbol{IF}^{m_{\beta_2}}$, yield feature vector $\boldsymbol{F}^{m_{\beta_1}}$ and $\boldsymbol{F}^{m_{\beta_2}}$

05. Feature evaluation by SVM

Compare Acc^{m_β}, $Acc^{m_{\beta_1}}$ and $Acc^{m_{\beta_2}}$

Output: the optimal frequency band and the best accuracy.

3. Experimental Research

3.1 Data Description and Preprocessing

The proposed method was first examined in detail based on a publicly available motor imagery dataset, which was provided by BCI Lab, Graz University of Technology. The datasets generated and analysed during the current study is available in the BCI Competition III Dataset IIIa repository, http://www.bbci.de/competition/iii.[44] After that, it was applied to a second motor imagery dataset which was acquired from a real-world experiment. The dataset is available from the corresponding author on reasonable request. For easy of description, the referenced datasets were renamed as Dataset A and Dataset B below.

3.1.1 Dataset A: BCI Competition III Dataset IIIa

The public EEG dataset considered originally consists of 60 EEG recordings referenced to the left mastoid and with the right mastoid serving as ground, the electrode position distribution is shown according to the scheme in Figure 1. EEG was sampled at 250 Hz, it was online filtered by a bandpass filter between 1 and 50Hz with Notch filter on to remove

artifacts. Data consists of three subjects performing imagined left hand and right hand movements. A training and a testing set are available for each subject. Both sets contain 45 trials per class for subject 1 (labeled as 'k3b'), and 30 trials per class for subjects 2 and 3 (labeled as 'k6b' and 'l1b'). The subjects sat in a comfortable chair with armrests and were instructed to perform a specific motor imagery task once the relevant cue was shown on a screen, until a fixation cross disappeared. Each trial lasted 8 seconds. After trial began, the first 2s were quiet, at t=2s an acoustic stimulus indicated the beginning of the trial, and a cross "+" was displayed; then from t=3s an arrow to the left or right was displayed for 1 s; at the same time the subject was asked to imagine a left hand or right hand movement, respectively, until the cross disappeared at t=7s. The subjects took a break and then conducted the next experiment. The MI-EEG collection timing scheme is shown in Figure 2.

For the preprocessing stage, spatial filtering using the method of common average reference was firstly applied. Each trial extracted from the time segment between 3.5 s and 7 s and was spectral filtered in α band (8-13Hz) and β band (13-30Hz) (If necessary, EEG signals would be filtered to β_1 (13-21Hz) and β_2 (21-30Hz) band as well). In order to reduce the computational complexity, 34 channel MI-EEG signals were selected symmetrically to carry out the experiment. Furthermore, the selected electrodes cover as many brain regions as possible. The choosing sensor numbers are: 1、2、3、4、5、7、9、11、13、15、17、19、21、23、25、27、29、31、33、35、37、39、41、43、45、47、49、51、53、55、57、58、59、60, respectively. Renumber these 34 channel MI-EEG signals as 1-34 for subsequent experimental research.

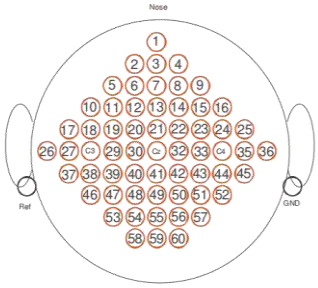

Figure 1. Electrode positions of Dataset A

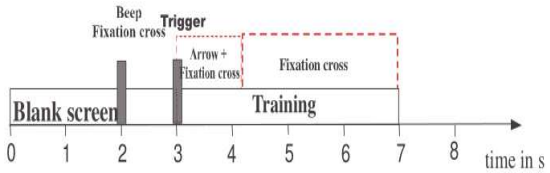

Figure 2. Timing diagram of Dataset A

3.1.2

Dataset B: Real acquisition data

The real acquisition MI-EEG data were acquired by Neuroscan EEG signal recording and analysis system. EEGs were collected using 64 Ag/AgCl electrodes placed according to the international 10-20 system. The subjects are 9 healthy graduate students aged between 23 and 26(marked as S1-S9, respectively), including two females and seven males. All of them are right-handed and without cognitive impairment. The MI tasks included imagining right-hand pronation and supination, and the sampling frequency was 1000 Hz. In order to ensure the quality of MI-EEG signals, the acquisition experiment of each subject was divided into 5 runs, one run consists of 20 trials (10 for each of two possible classes). Each subject should be trained in 2 runs of MI tasks before formal acquisition experiment to guarantee they

were familiar with the experimental process. Each trial lasted 8s, and the timing diagram is shown in Figure 3.The first 2s was the preparation period, the "+" cursor appeared on the screen; at t=2s the motor imagery prompt tone appeared, and the prompt video was displayed on the screen for 2 seconds, i.e., imagining the right-hand pronation or supination; the subject performed the corresponding MI task according to the video prompt at 4~8s; the end sound of MI task appeared on 8s, the subjects took a rest and then proceeded to the next experiment.

Thereafter, the original acquisition MI-EEG signals were down-sampled to 250 Hz and the ocular artifacts were removed. Then, a CAR spatial filter was used for baseline correction. The 4.5-7.5s MI-EEG was further intercepted and filtered to different frequency bands. Meanwhile, 28 channels are selected to reduce information redundancy and they are covered by red circles in Figure 4.

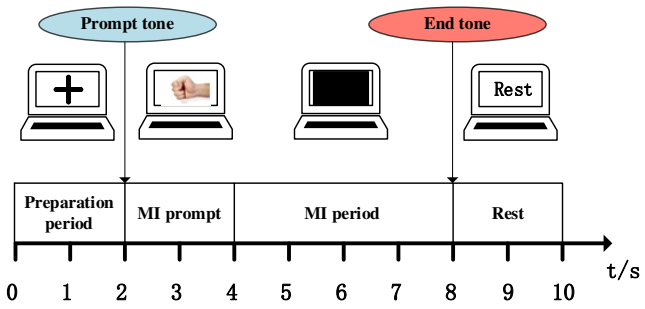

Figure3. Timing diagram of Dataset B

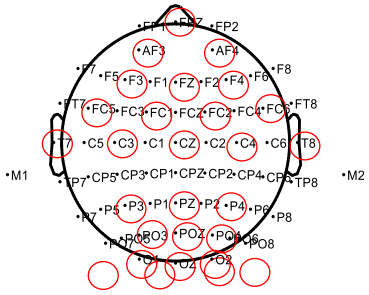

Figure4. The selected channels of Dataset B

3.2 Experimental results on Dataset A

3.2.1 Adaptive selection of the best frequency band and *m* values for each subject

For subject 'k3b', MVAR were fitted to the preprocessed MI-EEG data (both α and β band) and the model order of α and β band were p_α=3 and p_β=8, respectively. As is known to us all, the wider frequency band the signal, the more complex the signal is. Obviously, a higher model order is needed to match and describe the signal. Furthermore, $\boldsymbol{B}^{m_\alpha}(f)$ and $\mathbf{B}^{m_\beta}(f)$ were calculated according to Equation (6). Following the steps described in the Methods Section, features $\boldsymbol{F}^{m_\alpha}$ and $\boldsymbol{F}^{m_\beta}$ were finally acquired and then classified by SVM. For comparative studies, experiments were also carried on MI-EEG signals filtered to 8-30Hz with the model order of 10. The 10×10-fold cross validation (CV) methodology was used in this paper to eliminate the contingency in feature extraction process of MI-EEG signals as well as increase reliability of the experimental results, i.e., it uses nine observations to train the classifiers and the remaining one for testing the model. The final classification accuracy is the average of the 10 runs [45], as is shown in Figure 5(a) and *m* refers to the varying model order in the subsequent sections.

It can be clearly seen from Figure 5(a) that the highest recognition rate without frequency band selection, i.e., 91.67%, is lower than 96.78%, which is the best accuracy after band selection. In addition, classification accuracies in β band are always higher than that in α band. Considering β band is broader and may contain redundant information, it is necessary to refine it and find the most active band for recognition. Under this consideration, we separated β band into 2 subbands, i.e., β_1 band or lower β band (13-21Hz) and β_2 band or higher β band (21-30Hz). The same experiment was performed on MI-EEG signals in these two subbands, as is displayed in Algorithm. The model order of β_1 and β_2 band were 5 and final recognition rates were exhibited in Figure 5 (b) for better observations. In Figure 5(b), signals in β_2 band possess a higher degree of accuracy than that in β_1 band except for m is 1. Unbelievably and reasonably, identification rate reaches 100% when m is set to 2 in β_2 band.

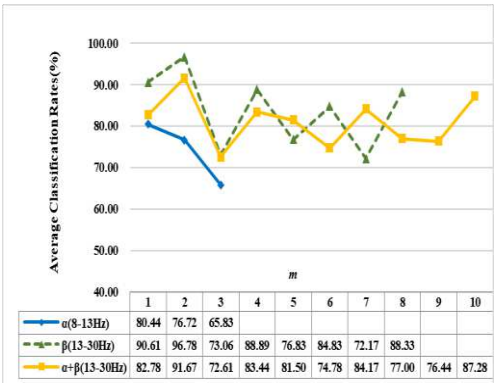

	1	2	3	4	5	6	7	8	9	10
α(8-13Hz)	80.44	76.72	65.83							
β(13-30Hz)	90.61	96.78	73.06	88.89	76.83	84.83	72.17	88.33		
α+β(13-30Hz)	82.78	91.67	72.61	83.44	81.50	74.78	84.17	77.00	76.44	87.28

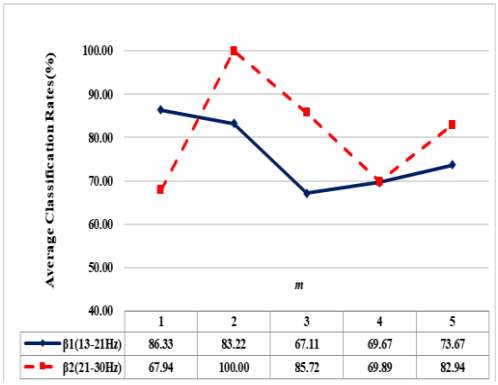

	1	2	3	4	5
β1(13-21Hz)	86.33	83.22	67.11	69.67	73.67
β2(21-30Hz)	67.94	100.00	85.72	69.89	82.94

(a) α, β and α+β band

(b) β_1 and β_2 band

Figure 5. Effects of different frequency bands and *m* values on the classification results for subject 'k3b'

The same operations were carried on subjects 'k6b' and 'l1b', average classification rates with 10×10-fold CV were demonstrated in Figure 6(a) for 'k6b' and Figure 6(b) for 'l1b', respectively.

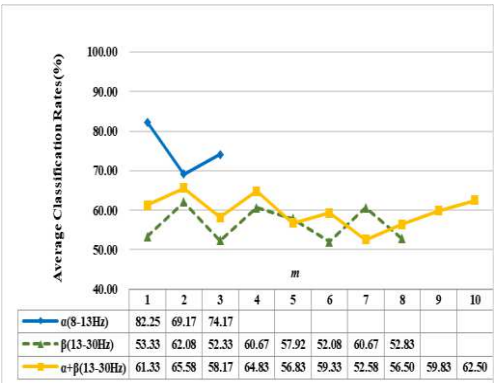

	1	2	3	4	5	6	7	8	9	10
α(8-13Hz)	82.25	69.17	74.17							
β(13-30Hz)	53.33	62.08	52.33	60.67	57.92	52.08	60.67	52.83		
α+β(13-30Hz)	61.33	65.58	58.17	64.83	56.83	59.33	52.58	56.50	59.83	62.50

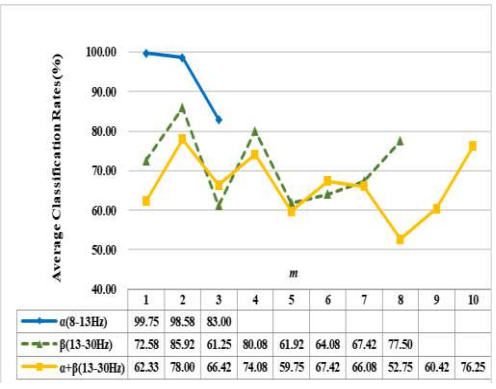

	1	2	3	4	5	6	7	8	9	10
α(8-13Hz)	99.75	98.58	83.00							
β(13-30Hz)	72.58	85.92	61.25	80.08	61.92	64.08	67.42	77.50		
α+β(13-30Hz)	62.33	78.00	66.42	74.08	59.75	67.42	66.08	52.75	60.42	76.25

(a)subject ‘k6b’ (b) subject ‘l1b’

Figure 6. Effects of different frequency bands and *m* values on the classification results for subjects‘k6b’and ‘l1b’.

Different from subject ‘k3b’, subjects ‘k6b’ and ‘l1b’ show better separability in α band comparing to β band under left-right hands motor imagery tasks. Nevertheless, subject ‘l1b’ performs better than ‘k6b’ and gets higher accuracies. This phenomenon perfectly tallies with subject-based characteristic of MI-EEG signals. Affected by internal and external environments, subjects show big diversities. Even for the same person, the recognition rates vary a lot in various frequency bands, as is shown in Figure 5(a) and5(b). Moreover, classification results of MI-EEG signals filtered to 8-30Hz are worse than those with adaptive frequency band selection (α band) for subjects ‘k6b’ and ‘l1b’. All the above reveals that dividing EEG signals into varying frequency bands could improve the classification performances.

Similarly, recognition rates get largely promoted when *m* is set to 1 or 2 instead of the original model order *p* despite in either frequency band for all the subjects. This is because MI-EEG signals are non-stationary in frequency domain, information of previous 1 or 2 moment is much more related to the current state and thus is more beneficial for recognition than taking all the information into account. According to Figure 5 and 6, MI-EEG signals in β band have similar recognition rates with the model order of 8 and 1 while classification rates reach the highest with the model order of 2, which suggests the frequency domain model obtained by Fourier transform of time domain model cannot truly reflect the variation characteristics of MI-EEG in frequency domain. Last but not least, the best frequency bands, *m* values and average classification rates with 10×10-fold CV for each subject are summarized in Table 1.

Table 1. Summarization of the best parameters for all subjects on Dataset A

Subjects	Best frequency bands	Best *m* values	Average classification rates with 10×10-fold
‘k3b’	β_2(21-30Hz)	2	100.00%
‘k6b’	α(8-13Hz)	1	82.25%
‘l1b’	α(8-13Hz)	1	99.75%

3.2.2 Classification rates without frequency band selection

In this section, the classification rates without frequency band selection for 3 subjects were displayed in Figure 7 for convenient observations.

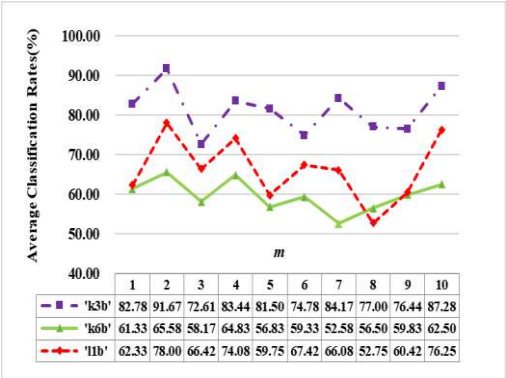

	1	2	3	4	5	6	7	8	9	10
'k3b'	82.78	91.67	72.61	83.44	81.50	74.78	84.17	77.00	76.44	87.28
'k6b'	61.33	65.58	58.17	64.83	56.83	59.33	52.58	56.50	59.83	62.50
'l1b'	62.33	78.00	66.42	74.08	59.75	67.42	66.08	52.75	60.42	76.25

Figure 7. Effects of different *m* values on the classification results in $\alpha + \beta$ band for each subject.

Comparing the results in Figure 7 with those in Figure 5 and 6, we can see the best results without frequency band selection for subjects 'k3b', 'k6b' and 'l1b'are 91.67%, 65.58% and 78.00%, respectively, which are much lower than 100.00%, 82.25% and 99.75% with frequency band selection. It further verifies that adaptive selection of the best frequency band for individual subject can improve the classification rates. In the meantime, it is observed that the best classification accuracies are achieved when *m* values were set to 2 for all the three subjects and this phenomenon coincides with the above ones. What's more, accuracies gain a certain degree of improvement ranging from 1.75% to 4.39% with selection of *m* values, which is lower than 8.33% ~17.06% with selection of both the best frequency band and *m* values. This indicates that the double selection of the best frequency band and *m* values for each person can yield the best results, which shows the effectiveness of DDTF.

3.2.3 Visualizations of adjacency matrices, brain functional networks and outflows

It is noted from the results in Section 3.2.1 and 3.2.2 that recognition rates get promoted when *m* equals to 1 or 2 in either frequency band for each person, so we take one trial of 'k3b' in α band for example to see the distinctions of adjacency matrices, brain functional networks and outflows under different *m* values. In addition, we denote 'LH' task as imagine left hand movement and 'RH' task as imagine right hand movement for convenient expressions.

The adjacency matrices under different *m* values for 'LH' and 'RH' tasks are expressed in Figure 8. Horizontal and vertical axis represent the new channel number, elements in the matrices reveal the direction and strength of information between two channels. The closer the color is to red, the higher the intensity. On the contrary, the closer the color is to blue, the lower the intensity. The corresponding brain functional networks based on graph theory are constructed with EEG electrodes as nodes and the adjacency matrices as links between channels, as are shown in Figure 9. In order to display the connectivity between channels

more clearly, the amount of interactions was limited by setting a threshold at 50% of the maximum matrix elements value. Several elements in adjacency matrices with higher intensities in Figure 8(a) and 8(d) correspond to the information transfers among channels shown in Figure 9(a) and 9(d). As is clearly seen from Figure 8 and 9 that with the increase of *m* values, information transfers get sharp augments. This suggests brain functional networks are in the transition from transient state to stable state.

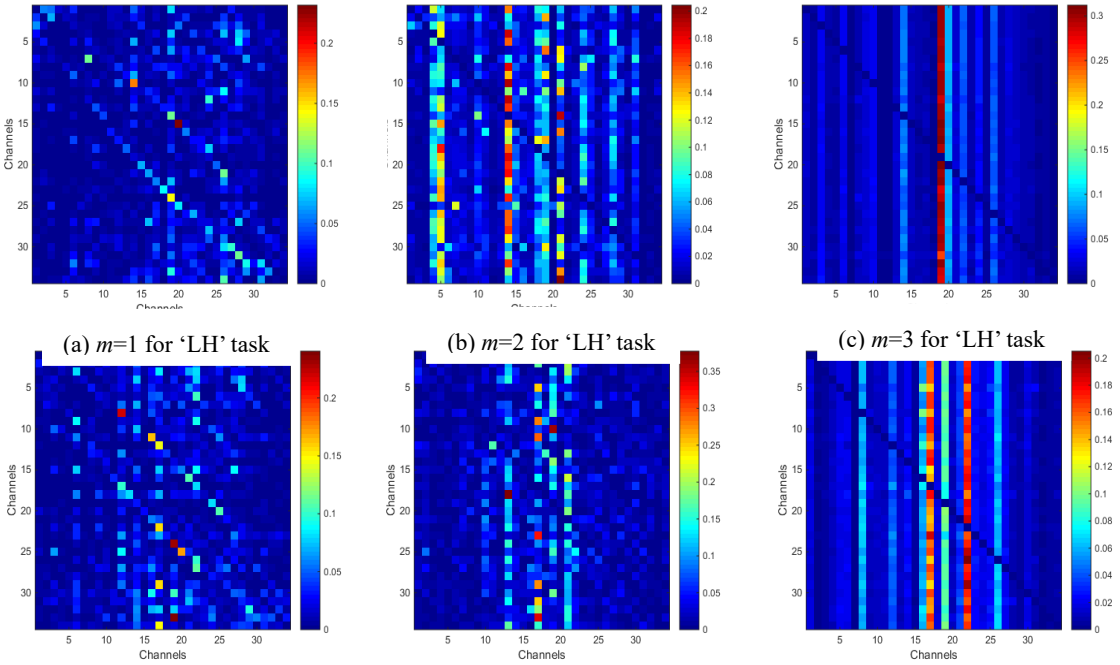

(a) *m*=1 for 'LH' task (b) *m*=2 for 'LH' task (c) *m*=3 for 'LH' task

(d) *m*=1 for 'RH' task (e) *m*=2 for 'RH' task (f) *m*=3 for 'RH' task

Figure 8. AMs of 'k3b' in α frequency band under different *m* values for 'LH' and 'RH' tasks

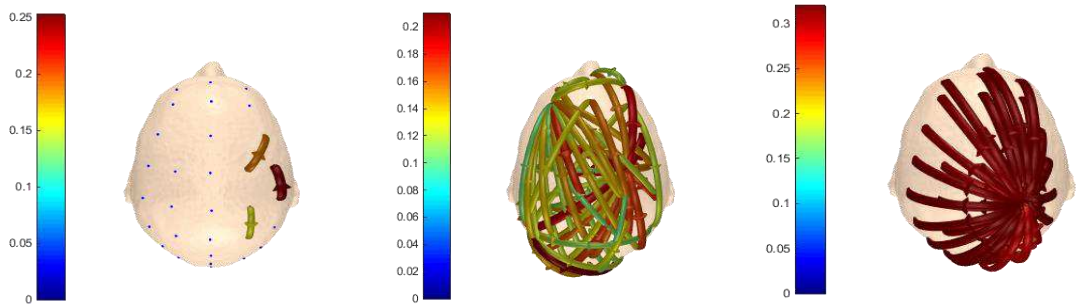

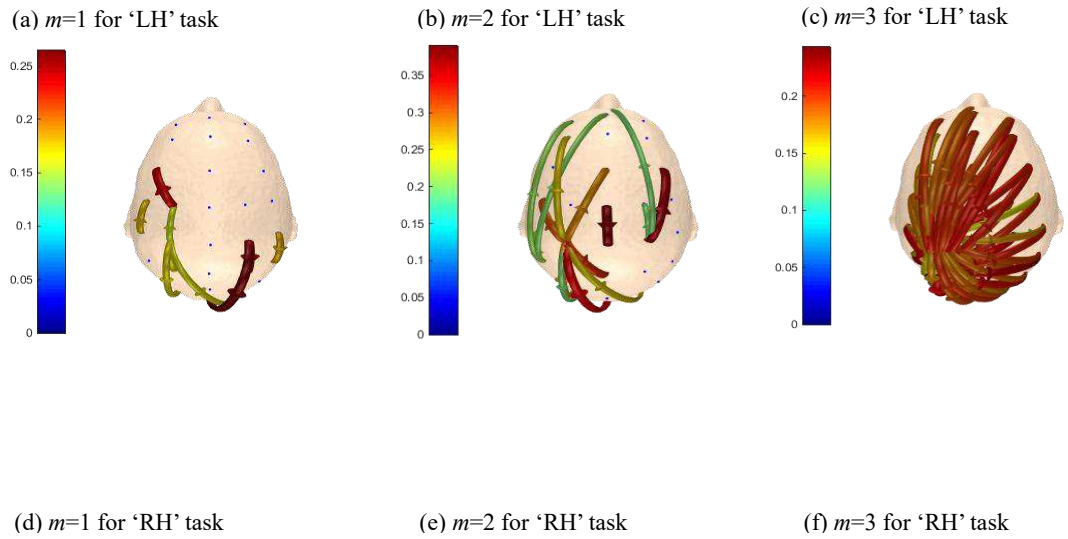

Figure 9. BFNs of 'k3b' in α frequency band under different m values for 'LH' and 'RH' tasks

Figure 10 demonstrates the outflows from all channels. Considering the spatial distribution of the networks, we can note from the figure that electrodes located in the central parietal area, which are reported to be related with somatosensory and motor activity [46-47], have larger outflows. Meanwhile, information originates mainly from right parts of the brain when imaging left hand movement and vice versa. It is generally accepted that the movement of the body is denominated by the contralateral part of the brain. The adjacency matrices, brain functional networks and outflows in β band of 'k3b' when m equals to 2 are also visualized in Figure 11 for comparison. It can be observed that there are considerable differences between α and β band, which further provides theoretical basis for our method.

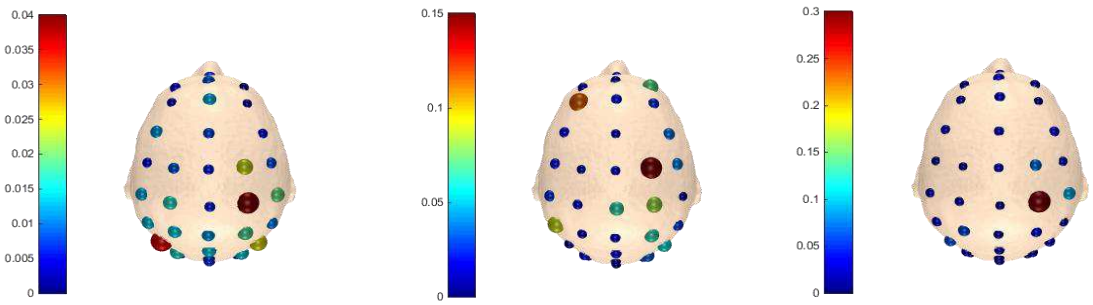

(a) *m*=1 for ‘LH’ task (b) *m*=2 for ‘LH’ task (c) *m*=3 for ‘LH’ task

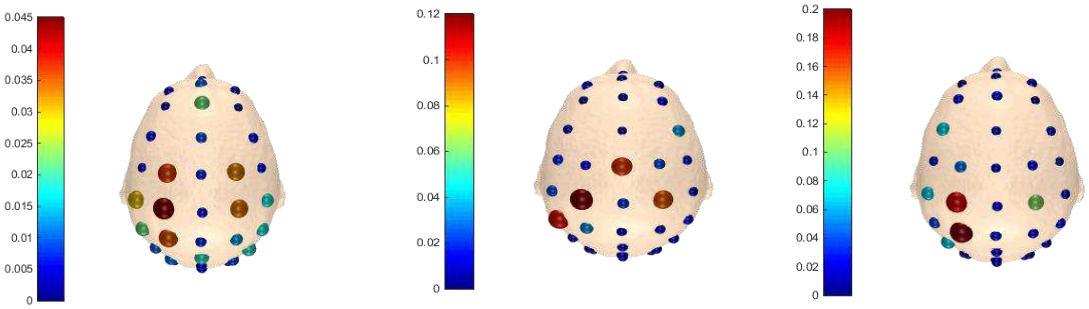

(d) *m*=1 for ‘RH’ task (e) *m*=2 for ‘RH’ task (f) *m*=3 for ‘RH’ task

Figure 10. Outflows of ‘k3b’ in α frequency band under different *m* values for ‘LH’ and ‘RH’ tasks

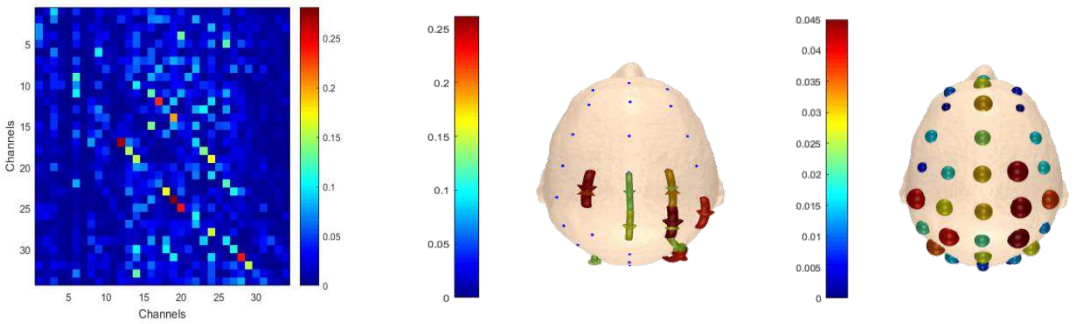

(a) AM for ‘LH’ task (b) BFN for ‘LH’ task (c) outflows for ‘LH’ task

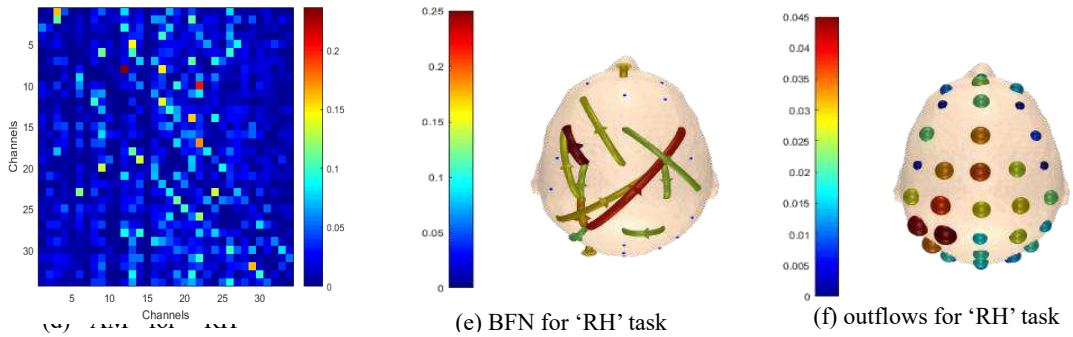

(d) AM for ‘RH’ task (e) BFN for ‘RH’ task (f) outflows for ‘RH’ task

Figure 11. AMs, BFNs and outflows of ‘k3b’ in β frequency band for ‘LH’ and ‘RH’ tasks

3.3 Experimental results on Dataset B

Aiming a better insight of potential performance in real acquisition data, DDTF is extended to Dataset B. Under the same experimental procedure in section 3.2, the 10×10-fold cross-validation classification accuracies were shown in Figure 12 when DDTF was applied to extract features from 9 subjects, and the best parameters for each subject are summarized in Table 2. It can be found from Figure 12 and Table 2 that the optimal frequency bands were varying for different subjects. Even for the same subject, the classification results over different frequency bands also had a huge disparity, which fully reflected the individual differences of MI-EEG. Therefore, the personalized selection of parameters will be helpful to improve the recognition rate for each subject. Not coincidentally, for each frequency band of all subjects, the recognition rates were greatly improved when m took 1 or 2 instead of the original order p, which was consistent with the conclusion of dataset A, and further validated the correctness and universality of DDTF.

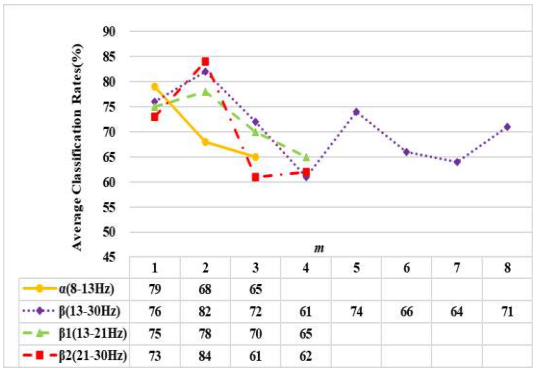

(a) S1

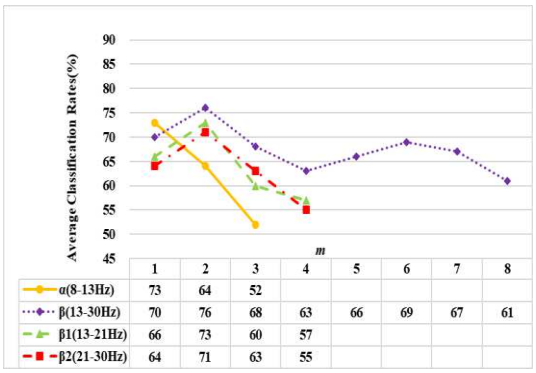

(b) S2

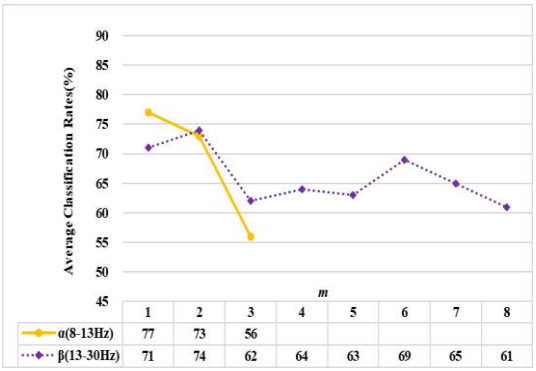

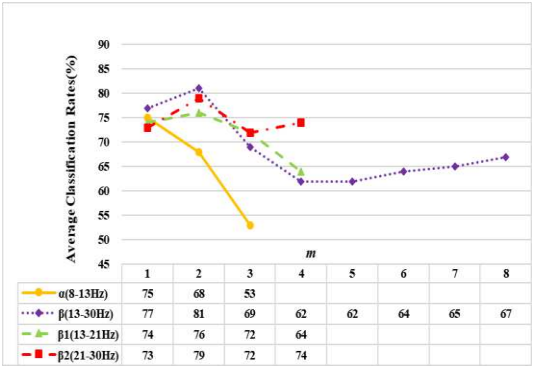

(c) S3

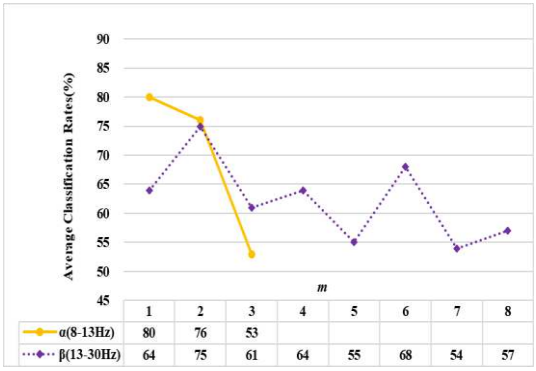

(d) S4

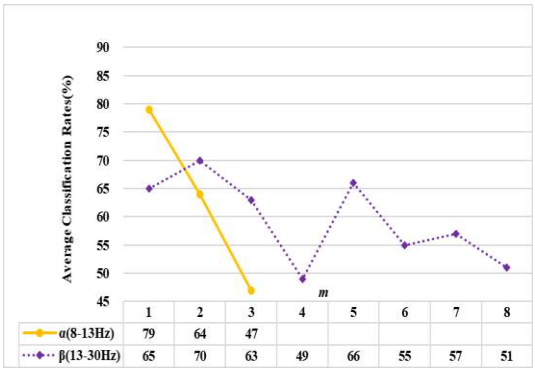

(e) S5

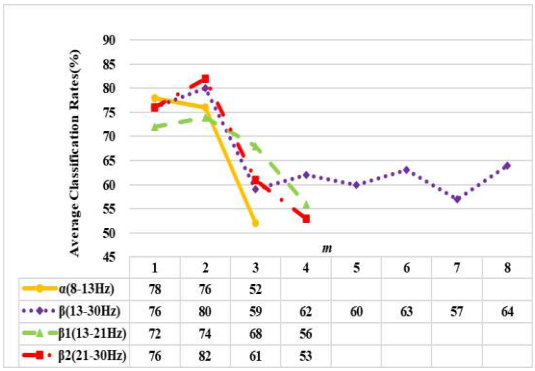

(f) S6

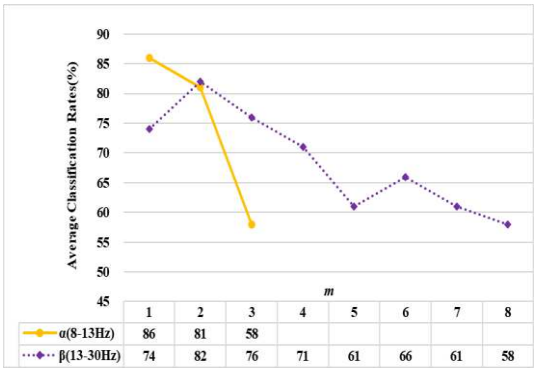

(g) S7

(h) S8

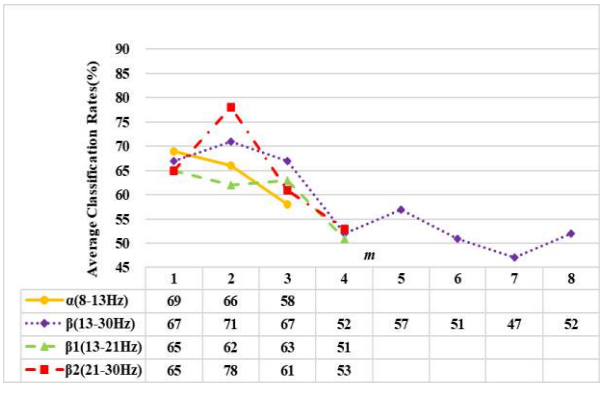

(i) S9

Figure 12. Effects of different frequency bands and *m* values on the classification results for all subjects on Dataset B

Table 2. Summarization of the best parameters for all subjects on Dataset B

Subjects	Best frequency bands	Best *m* values	Average classification rates with 10×10-fold
S1	β_2(21-30Hz)	2	84%
S2	β(13-30Hz)	2	76%
S3	α(8-13Hz)	1	77%
S4	β(13-30Hz)	2	81%
S5	α(8-13Hz)	1	80%
S6	α(8-13Hz)	1	79%
S7	β_2(21-30Hz)	2	82%
S8	α(8-13Hz)	1	86%
S9	β_2(21-30Hz)	2	78%

3.4. Comparative experiments on Dataset A

3.4.1 Comparison with GC-based brain functional network methods on Dataset A

To verify the validity of DDTF, the comparative experiments among DDTF and GC-based brain functional network methods were carried out. GC-based BFN methods were applied to MI-EEG signals filtered to 8-30Hz and SVM was applied as the classifier. The average recognition results of 10×10-fold CV are displayed in Figure 13.

From Figure 13, it's easy to see that Time-domain GC(TGC) has a not very good average classification performance. This is mainly because this method only considers the interactions in time domain while ignoring the spectral properties of MI-EEG signals. Frequency-domain GC(FGC) uses both time and frequency information, which yields a slightly higher accuracy. However, these two methods just focus on information flow between two channels without considering the integrality of the whole brain. Despite the results of TGC and FGC being poor,

DTF shows the advantages of multivariate autoregressive methods over traditional univariate methods for each subject in terms of classification accuracy. In addition, for each subject, the recognition rates obtained by using DDTF to extract features of MI-EEG are significantly enhanced than those of DTF. The time domain model and frequency domain model share the same model order in DTF, however, the frequency domain model can't truly be used to construct and embody the changes of MI-EEG brain functional networks. Moreover, individual differences of allied cognitive tasks are observed in DDTF, which produces better quality information. For different subjects, our method achieved better recognition accuracy than the above GC-based methods, indicating the superiority of DDTF.

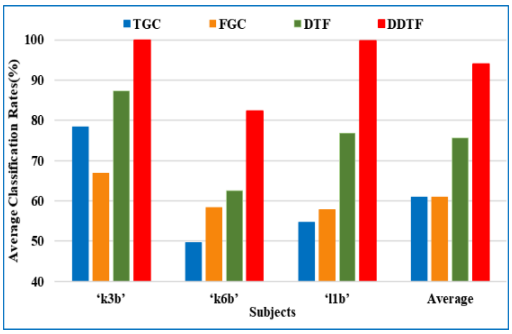

Figure 13. Comparison of average classification rates with GC-based BFN methods on Dataset A.

3.4.2 Statistical Analysis

(1) Kappa coefficient

In this section, more statistical analysis was executed to confirm the effectiveness of DDTF. The kappa coefficient, which is generally thought to be a more robust measure than simple percent agreement calculation, takes into account the agreement occurring by chance. It is a common indicator for evaluating the performance of BCI systems [48]. The calculation of kappa coefficient is defined as:

$$k = \frac{p_0 - p_e}{1 - p_e} \tag{18}$$

where p_0 indicates the classification accuracy, p_e represents the probability of opportunity consistency. For a two-class task, if the number of samples across classes is equal, then the value of p_e is 0.5. According to equation (18), the kappa coefficients of TGC, FGC, DTF as well as DDTF with 10×10-fold CV were calculated. The results are shown in Figure 14.

The kappa values illustrated in Figure 14 indicate that DDTF gets the highest improvement for all the subjects. It is worth noting that the kappa value increased from 0.25 to 0.64 for subject 'k6b' and from 0.54 to 0.99 for subject 'l1b', respectively. Although there

are variations in kappa values for each subject, the mean kappa value of DDTF is improved by 0.37 compared to the DTF method, which reveals that DDTF has better consistency in classification. Furthermore, the mean value of DDTF is 0.88, which is higher than 0.8, illuminates a very good level of agreement.

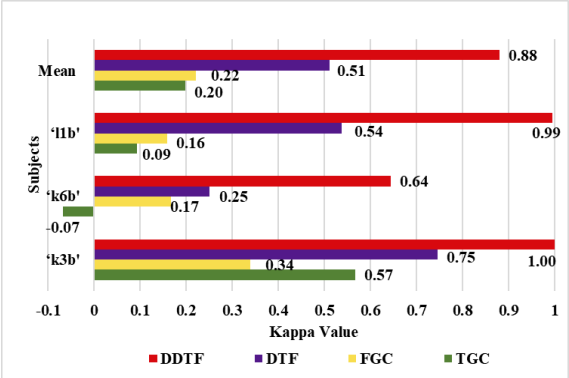

Figure 14. Comparison of Kappa coefficients with GC-based brain functional network methods.

(2) t-test

To further analyze the differences between DTF and DDTF statistically, a two-sample *t*-test is proceeded to inspect whether there is a significant difference when they are available for MI-EEG feature extraction. Suppose that $\bar{M}_{DTF}$ and $\bar{M}_{DDTF}$ denote the mean values of 10-fold CV accuracies generated by DTF and DDTF, similarly, ${S^2}_{DTF}$ and ${S^2}_{DDTF}$ stand for the variance, n_{DTF} and n_{DDTF} express the number of the results for the two methods, respectively. Then, the *t*-test statistic is calculated as follows:

$$t = \frac{\bar{M}_{DDTF} - \bar{M}_{DTF}}{\sqrt{\frac{(n_{DDTF}-1){S^2}_{DDTF} + (n_{DTF}-1){S^2}_{DTF}}{n_{DDTF}+n_{DTF}-2}\left(\frac{1}{n_{DDTF}} + \frac{1}{n_{DTF}}\right)}} \tag{19}$$

Define the null hypothesis is H_0: the results of DTF and DDTF originate from independent random samples from normal distributions with equal means; the alternative hypothesis is H_1: the results of DTF and DDTF come from populations with unequal means. The significance level is set as $\mu = 0.05$. The decision rule is to reject H_0, if:

$$p = \mathrm{P}\{t > t_{\mu}(n_{DDTF} + n_{DTF-2})\} \leq 0.05 \tag{20}$$

It can be calculated that the values of p for 3 subjects are 2.0402×10^{-16}, 3.0029×10^{-22} and 4.8337×10^{-19}, respectively, and they are all less than 0.05. Hence, the null hypothesis H_0 is rejected at the 0.05 significance level, which implies DDTF outperforms DTF in MI-EEG

feature extraction.

3.4.3 Comparison with Multiple Traditional Feature Extraction Methods

CSP and its variants have been widely studied in feature extraction of MI-EEG on BCI competition III and gained good recognition results. To further illustrate the feasibility of DDTF in this paper, the comparison experiments with multiple CSP-based methods in references **Error! Reference source not found.**-9] were executed. Table 3 illustrates the detailed information. It can be seen that DDTF achieves the highest recognition rate of 100.00% and 99.75% for subjects 'k3b' and 'l1b', respectively, and the average classification accuracy, i.e., 94.00%, is superior to the best one with 91.87% in the CSP-based feature extraction methods. The variants of CSP methods extract features under the consideration of multi-channel and spatial distribution characteristics of MI-EEG signals while pitifully neglecting the relationships among EEG sensors. DDTF effectively excavates the interrelationship between multi-channel EEG signals, correctly analyzed the information exchange over the whole brain, and had better applicability in extracting features from MI-EEG signals.

Table 3. Comparison with multiple CSP-based feature extraction methods

Reference number	Methods	Subjects			Average accuracies (%)
		'k3b'	'k6b'	'l1b'	
[7]	AC-CSP	97.80	63.30	94.20	85.10
[7]	AC-RCSP	97.80	72.50	95.00	88.43
[7]	CCS-CSP	98.90	79.20	95.80	91.30
[7]	CCS-RCSP	98.90	80.00	96.70	91.87
[8]	CSSSP	95.50	55.10	95.00	81.87
[8]	BCSP	78.80	63.70	76.60	73.03
[8]	ACSP	76.60	56.80	51.60	61.67
[8]	Pcv	**100.00**	68.90	96.60	88.50
[8]	Pfix	**100.00**	67.20	98.30	88.50
[9]	CSP	67.50	70.00	53.30	63.60
[9]	CCSP	95.00	**90.00**	83.30	89.43
This Paper	DDTF	**100.00**	82.25	**99.75**	**94.00**

Note: Pcv and Pfix represent the CCSSP with and without automatic parameter selection, respectively.

3.5 Comparative experiments on dataset B

In this section, DDTF was compared with the original DTF and GC-based BFN methods on dataset B, some relative experiments were performed and the results were shown in Figure 15 and Table 4, respectively. It can be seen from Figure 15 that for each subject, the classification accuracy of DTF is significantly higher than that of TGC, FGC and DTF when used for MI-EEG feature extraction. The average classification accuracy of DDTF makes

14% improvement over DTF, where S6 gets the highest, i.e., 26%. The Kappa coefficients in Table 4 show that DDTF has varying degrees of improvement for 9 subjects, and the average Kappa value of DDTF is 0.61, which has an increase of 0.31, 0.41 or 0.38 compared with DTF, TGC or FGC, respectively, revealing that DDTF has the best consistency.

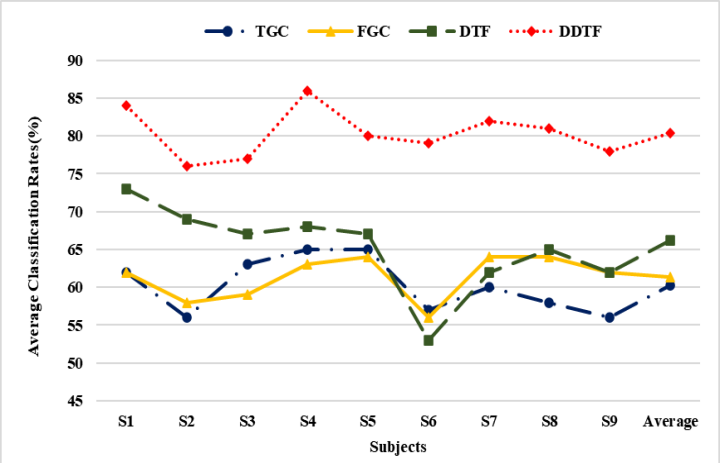

Figure 15. Comparison of average classification rates with GC-based BFN methods on Dataset B.

Table 4. Comparison of Kappa coefficients with GC-based BFN methods on Dataset B.

Methods	Subjects									Average
	S1	S2	S3	S4	S5	S6	S7	S8	S9	
TGC	0.24	0.12	0.26	0.16	0.30	0.14	0.20	0.30	0.12	0.20
FGC	0.24	0.16	0.18	0.28	0.28	0.12	0.28	0.26	0.24	0.23
DTF	0.46	0.38	0.34	0.30	0.34	0.06	0.24	0.36	0.24	0.30
DDTF	0.68	0.52	0.54	0.62	0.60	0.58	0.64	0.72	0.56	0.61

4. Discussion

In this paper, DDTF was proposed for brain functional network based feature extraction. In DDTF, the optimal frequency band for each subject is adaptively selected, which preferably detects the subject-based feature of MI-EEG and $\boldsymbol{B}^m(f)$ is defined with a varying order m. The adaptive selection of the best frequency band for individual subject can improve the classification rates. In addition, the best classification accuracies in either frequency band for each subject are achieved when m values equals 1 or 2. To seek for the reasons, we took subject 'k3b' on Dataset A for example and drew the changing curves of channels 27 and 35

MI-EEG signals in time and frequency domains, which were illustrated as Figure 16. Figure 16 (a) to Figure 16 (e) show the variation of channels 27 and 35 in time and frequency domains when filtered to $\alpha, \beta, \beta_1, \beta_2$ and $\alpha+\beta$ frequency bands, respectively. As is known us all, MI-EEG signals have approximate stationary over short time intervals when the MVAR model is constructed in time domain. Therefore, the time domain MVAR model can express the changes of time domain signals correctly. However, the non-stationarity of frequency domain signals becomes very intense because of the activated features generated by motor imagery in either α or β frequency band, which can be clearly seen from Figure 16. Although DTF can correctly reflect the quantitive relationships between the time and frequency domain model, it may not effectively express the characteristics of the frequency domain MI-EEG signals. Then, further than that, we constructed the frequency domain MVAR model based on the MI-EEG filtered to α band and got the model order of 1, the results perfectly match the non-stationarity of MI-EEGs in frequency domain. In [27-28], the time domain model and frequency domain model share the same model order, which ignores the non-stationarity of frequency domain signals. Particularly, DDTF is the same as DTF [27-28] when m_α equals to p_α while DDTF can represent the variation characteristics of MI-EEG in frequency domain and the brain functional networks constructed by DDTF are more veritable and objective. The same experiments were also carried on other subjects and we got similar conclusions.

The adjacency matrices and brain functional networks in Figure 8 and 9 show that with the increase of m values, information transfers get sharp augments and brain functional networks are in the transition from transient state to stable state. Figure 10 indicates the electrodes having larger outflows are located in the central parietal area which are related with motor activity and information originates mainly from right parts of the brain when imaging left hand movement and vice versa, which is in accordance with the well-accepted theory. What is said above further provided theoretical support for our method.

In addition, DDTF were compared with GC-based BFN feature extraction methods, and DDTF achieved the highest average classification accuracies of 12 subjects, as is shown in Figure 13 and Figure15. The kappa coefficients of TGC, FGC, DTF and DDTF were calculated for statistical analysis. The results in Figure 14 and Table 2 illustrate that DDTF had better consistency in classification than the other three methods. Besides, a two-sample *t*-test statistic was designed to explore whether there was a significant difference between DTF and DDTF in MI-EEG feature extraction. The results implied the superiority and feasibility of DDTF for brain functional network based feature extraction. This provided a new idea for extracting the features of MI-EEG as well as enhancing the adaptivity of feature extraction.

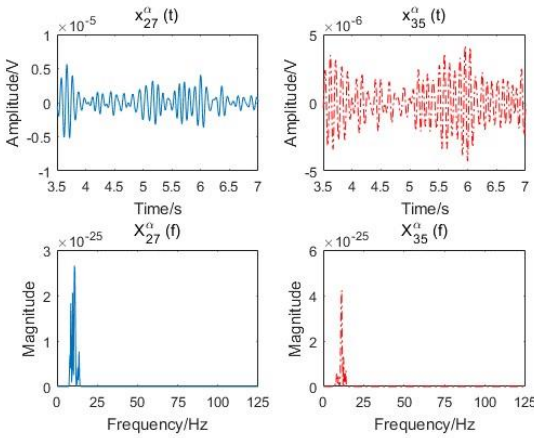

(a) the variations of channels 27 and 35 in time and frequency domains when filtered to α band

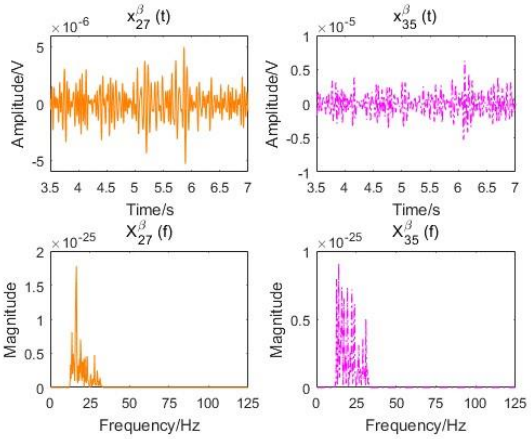

(b) the variations of channels 27 and 35 in time and frequency domains when filtered to β band

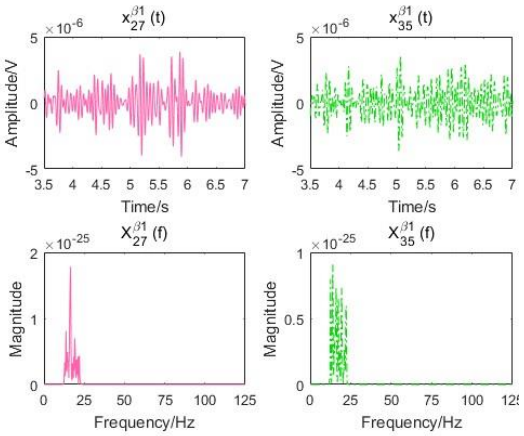

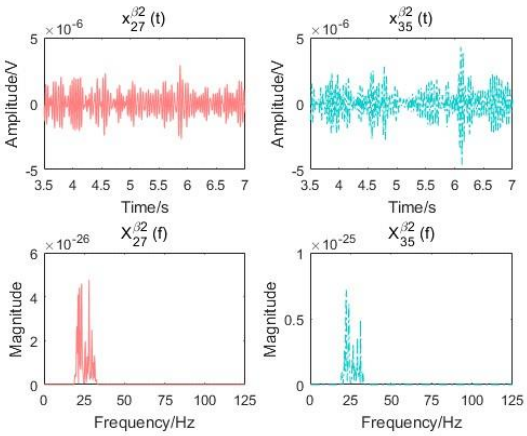

(c) the variations of channels 27 and 35 in time and frequency domains when filtered to β_1 band

(d) the variations of channels 27 and 35 in time and frequency domains when filtered to β_2 band

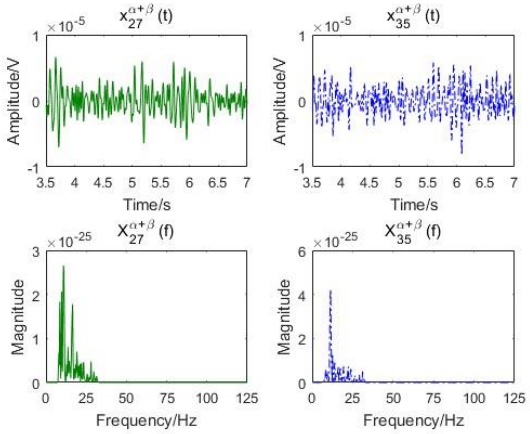

(e) the variations of channels 27 and 35 in time and frequency domains when filtered to $\alpha + \beta$ y band

Figure 16. the variation of channels 27 and 35 in time and frequency domains filtered to different frequency bands

5. Conclusions

A dynamic DTF, called DDTF, was developed in this study. It is calculated based on a dynamic frequency domain model with a lower order, and only the most related information is beneficial for recognition of MI-EEG, i.e., the previous 1 or 2 moment is much more related to the current state, and the brain functional network changes from transient state to stable state with the increment of model order. Meanwhile, the best frequency band can be adaptively sought for each individual. This makes it more closely coincident with the subject-based characteristic of MI-EEG, yielding better features and recognition rates. Extended experimental results have suggested that DDTF achieves excellent performance in brain functional network based feature extraction. In the future study, we intend to integrate the DDTF based brain functional network with other feature extraction methods to improve its property. In addition, it will provide a good prospect for disease diagnosis, seizure detection and rehabilitation effect evaluation.

Ethics approval and consent to participate

Not applicable.

Consent for publication

All authors of the manuscript have read and agreed the final manuscript.

Availability of data and materials

The Dataset A generated and analysed during the current study is available in the BCI Competition III Dataset IIIa repository, http://www.bbci.de/competition/iii.

The Dataset B used and analysed during the current study is available from the corresponding author on reasonable request.

Competing interests

The authors declare that they have no competing interests.

Funding

This work was supported by the National Natural Science Foundation of China under grant numbers No. 11882003 and No. 81471770.

Authors' contributions

The manuscript was produced, reviewed, and approved by all of the authors collectively. Mingai Li and Na Zhang contributed as first author and senior/last author, respectively. All authors read and approved the final manuscript.

Acknowledgements

We would like to thank the provider of dataset and all of the people who have given us helpful suggestions and advice. The authors are obliged to the anonymous referee for carefully looking over the details and for useful comments which improved this paper.

References

[1] Wolpaw J R, Birbaumer N, McFarland D J, et al. Brain–computer interfaces for communication and control[J]. Clinical neurophysiology, 2002, 113(6): 767-791.

[2] Ang K K, Guan C. EEG-based strategies to detect motor imagery for control and rehabilitation[J]. IEEE Transactions on Neural Systems and Rehabilitation Engineering, 2016, 25(4): 392-401.

[3] Li M, Xi H, Sun Y. Feature Extraction and Visualization of MI-EEG with L-MVU Algorithm[C]//World Congress on Medical Physics and Biomedical Engineering 2018. Springer, Singapore, 2019: 835-839.

[4] Blankertz B, Müller K R, Curio G, et al. The BCI competition 2003[J]. IEEE Trans. Biomed. Eng, 2004, 51(6): 1044-1051.

[5] Blankertz B, Muller K R, Krusienski D J, et al. The BCI competition III: Validating alternative approaches to actual BCI problems[J]. IEEE transactions on neural systems and rehabilitation engineering, 2006, 14(2): 153-159.

[6] Falzon O, Camilleri K P, Muscat J. Complex-valued spatial filters for task discrimination[C]//2010 Annual

International Conference of the IEEE Engineering in Medicine and Biology. IEEE, 2010: 4707-4710.

[7] Jin, Jing, et al. "Correlation-based channel selection and regularized feature optimization for MI-based BCI." Neural Networks 118 (2019): 262-270.

[8] Yu K, Wang Y, Shen K, et al. The Synergy between complex channel-specific FIR filter and spatial filter for single-trial eeg classification[J]. PloS one, 2013, 8(10): e76923.

[9] Li L, Xu G, Xie J, et al. Classification of single-trial motor imagery EEG by complexity regularization[J]. Neural Computing and Applications, 2019, 31(6): 1959-1965.

[10] McEvoy L K, Smith M E, Gevins A. Dynamic cortical networks of verbal and spatial working memory: effects of memory load and task practice[J]. Cerebral cortex (New York, NY: 1991), 1998, 8(7): 563-574.

[11] Li F, Tian Y, Zhang Y, et al. The enhanced information flow from visual cortex to frontal area facilitates SSVEP response: evidence from model-driven and data-driven causality analysis[J]. Scientific reports, 2015, 5: 14765.

[12] Li F, Liu T, Wang F, et al. Relationships between the resting-state network and the P3: Evidence from a scalp EEG study[J]. Scientific reports, 2015, 5: 15129.

[13] Zhang Y, Xu P, Guo D, et al. Prediction of SSVEP-based BCI performance by the resting-state EEG network[J]. Journal of neural engineering, 2013, 10(6): 066017.

[14] Zhang T, Liu T, Li F, et al. Structural and functional correlates of motor imagery BCI performance: Insights from the patterns of fronto-parietal attention network[J]. Neuroimage, 2016, 134: 475-485.

[15] Li F, Chen B, Li H, et al. The time-varying networks in P300: a task-evoked EEG study[J]. IEEE Transactions on Neural Systems and Rehabilitation Engineering, 2016, 24(7): 725-733.

[16] Wang G, Sun Z, Tao R, et al. Epileptic seizure detection based on partial directed coherence analysis[J]. IEEE journal of biomedical and health informatics, 2015, 20(3): 873-879.

[17] Van Mierlo P, Papadopoulou M, Carrette E, et al. Functional brain connectivity from EEG in epilepsy: Seizure prediction and epileptogenic focus localization[J]. Progress in neurobiology, 2014, 121: 19-35.

[18] Takigawa M, Wang G, Kawasaki H, et al. EEG analysis of epilepsy by directed coherence method a data processing approach[J]. International journal of psychophysiology, 1996, 21(2-3): 65-73.

[19] Wang J, Wang X, Xia M, et al. GRETNA: a graph theoretical network analysis toolbox for imaging connectomics[J]. Frontiers in human neuroscience, 2015, 9: 386.

[20] Friston K J. Functional and effective connectivity in neuroimaging: a synthesis[J]. Human brain mapping, 1994, 2(1‐2): 56-78.

[21] Ahmadi N , Pei Y , Carrette E , et al. EEG-based classification of epilepsy and PNES: EEG microstate and functional brain network features[J]. Brain Informatics, 2020, 7(1).

[22] Yao Z , Hu B , Xie Y , et al. A review of structural and functional brain networks: small world and atlas[J]. Brain Informatics, 2015, 2(1):45-52.

[23] Wiener N. The theory of prediction. Modern mathematics for engineers[J]. New York, 1956: 165-190.

[24] Granger C W J. Investigating causal relations by econometric models and cross-spectral methods[J]. Econometrica: Journal of the Econometric Society, 1969: 424-438.

[25] Geweke J. Measurement of linear dependence and feedback between multiple time series[J]. Journal of the American statistical association, 1982, 77(378): 304-313.

[26] Bastos A M, Schoffelen J M. A tutorial review of functional connectivity analysis methods and their interpretational pitfalls[J]. Frontiers in systems neuroscience, 2016, 9: 175.

[27] Kaminski M J, Blinowska K J. A new method of the description of the information flow in the brain structures[J]. Biological cybernetics, 1991, 65(3): 203-210.

[28] Kamiński M, Ding M, Truccolo W A, et al. Evaluating causal relations in neural systems: Granger causality, directed transfer function and statistical assessment of significance[J]. Biological cybernetics, 2001, 85(2): 145-157.

[29] Ding M, Bressler S L, Yang W, et al. Short-window spectral analysis of cortical event-related potentials by adaptive multivariate autoregressive modeling: data preprocessing, model validation, and variability assessment[J]. Biological cybernetics, 2000, 83(1): 35-45.

[30] Ginter J, Blinowska K J, Kaminski M, et al. Propagation of brain electrical activity during real and imagined motor task by directed transfer function[C]//Conference Proceedings. 2nd International IEEE EMBS Conference on Neural Engineering, 2005. IEEE, 2005: 105-108.

[31] Yi W, Zhang L, Wang K, et al. Evaluation and comparison of effective connectivity during simple and compound limb motor imagery[C]//2014 36th Annual International Conference of the IEEE Engineering in Medicine and Biology Society. IEEE, 2014: 4892-4895.

[32] Korzeniewska A, Mańczak M, Kamiński M, et al. Determination of information flow direction among brain structures by a modified directed transfer function (dDTF) method[J]. Journal of neuroscience methods, 2003, 125(1-2): 195-207.

[33] Billinger M, Brunner C, Müller-Putz G R. Single-trial connectivity estimation for classification of motor imagery data[J]. Journal of neural engineering, 2013, 10(4): 046006.

[34] Heger D, Terziyska E, Schultz T. Connectivity based feature-level filtering for single-trial eeg bcis[C]//2014 IEEE International Conference on Acoustics, Speech and Signal Processing (ICASSP). IEEE, 2014: 2064-2068.

[35] Wilke C, Ding L, He B. Estimation of time-varying connectivity patterns through the use of an adaptive directed transfer function[J]. IEEE transactions on biomedical engineering, 2008, 55(11): 2557-2564.

[36] Li F, Chen B, Li H, et al. The time-varying networks in P300: a task-evoked EEG study[J]. IEEE Transactions on Neural Systems and Rehabilitation Engineering, 2016, 24(7): 725-733.

[37] Li F, Peng W, Jiang Y, et al. The dynamic brain networks of motor imagery: time-varying causality analysis

of scalp EEG[J]. International journal of neural systems, 2019, 29(01): 1850016.

[38] Wang D, Ren D, Li K, et al. Epileptic seizure detection in long-term EEG recordings by using wavelet-based directed transfer function[J]. IEEE Transactions on Biomedical Engineering, 2018, 65(11): 2591-2599.

[39] Vanhatalo S, Voipio J, Kaila K. Full-band EEG (fbEEG): a new standard for clinical electroencephalography[J]. Clinical EEG and neuroscience, 2005, 36(4): 311-317.

[40] Millan J R. On the need for on-line learning in brain-computer interfaces[C]//2004 IEEE International Joint Conference on Neural Networks (IEEE Cat. No. 04CH37541). IEEE, 2004, 4: 2877-2882.

[41] Wu J, Srinivasan R, Kaur A, et al. Resting-state cortical connectivity predicts motor skill acquisition[J]. Neuroimage, 2014, 91: 84-90.

[42] Knight R T. Neural networks debunk phrenology[J]. Science, 2007, 316(5831): 1578-1579.

[43] Schwarz G. Estimating the dimension of a model[J]. The annals of statistics, 1978, 6(2): 461-464.

[44] BCI Competition III, Available: http://www.bbci.de/competition/iii.

[45] Santamaria L, James C. Use of graph metrics to classify motor imagery based BCI[C]//2016 International Conference for Students on Applied Engineering (ICSAE). IEEE, 2016: 469-474.

[46] Angulo-Sherman I N, Gutiérrez D. A link between the increase in electroencephalographic coherence and performance improvement in operating a brain-computer interface[J]. Computational intelligence and neuroscience, 2015, 2015: 67.

[47] Babiloni C, Brancucci A, Vecchio F, et al. Anticipation of somatosensory and motor events increases centro-parietal functional coupling: an EEG coherence study[J]. Clinical Neurophysiology, 2006, 117(5): 1000-1008.

[48] She Q, Ma Y, Meng M, et al. Multiclass posterior probability twin svm for motor imagery EEG classification[J]. Computational Intelligence and Neuroscience, 2015, 2015: 95.